From Vesicle Size Distributions to Bilayer Elasticity via Cryo-Transmission and Freeze-Fracture Electron Microscopy

B. Coldren, R. van Zanten, M. J. Mackel, and J. A. Zasadzinski*

Department of Chemical Engineering and Materials Research Laboratory, University of California, Santa Barbara, California 93106-5080

Hee-Tae Jung

Department of Chemical and Biochemical Engineering, Korea Advanced Institute of Science & Technology, 373-1 Guseong-dong, Yuseong-gu, Daejon 305-701, Korea

Received February 21, 2003. In Final Form: April 18, 2003

Three methods of evaluating vesicle mean radii and polydispersity, quasi-elastic light scattering (QLS), freeze-fracture electron microscopy (FF-TEM), and cryo-transmission electron microscopy (cryo-TEM), were used to determine the size distributions of spontaneous vesicles made from mixtures of cetyltrimethylammonium tosylate (CTAT) and sodium dodecylbenzene sulfonate (SDBS). While QLS is probably the most commonly used method to size vesicles, it is limited to measures of the mean hydrodynamic radius and an estimate of the polydispersity, both of which are heavily weighted toward the largest structures in the solution. Cryo-TEM can provide the entire size distribution of the outer diameters of spherical vesicles, from which the sum of the Helfrich bilayer elastic parameters, $K = \kappa + \bar{\kappa}/2$ and the spontaneous curvature radius, R_0, can be determined. FF-TEM can provide the number-average mean diameter and polydispersity once the influence of the fracture plane has been factored into the distribution, thereby confirming the cryo-TEM size distribution. For 7:3 wt CTAT/SDBS at 1% total surfactant in water, $K = \kappa + \bar{\kappa}/2 = 0.15 \pm 0.03\ k_BT$ and $R_0 = 55$ nm $\pm$ 10 nm. For CTAT/SDBS, w/w, at 2% total surfactant, $K = 0.54\ kT \pm 0.05\ k_BT$ and $R_0 = 36$ nm $\pm$ 1 nm. We find that surfactant mixing is likely the origin of the low bilayer elasticity in catanionic vesicles. However, the lower value of K in the CTAT-rich sample is likely due to the hydrophobic tosylate counterion increasing the area per headgroup.

Introduction

Particle size distribution, mean diameter, and polydispersity are important experimental parameters describing a colloidal dispersion. For self-assembled structures such as equilibrium vesicles, the size distribution is intimately related to characteristic bilayer parameters including the spontaneous curvature,[1,2] the Helfrich elastic moduli,[1−4] or even molecular parameters such as the extended length of a surfactant chain, the area per headgroup, and so forth.[4−8] While a number of theoretical vesicle size distributions are available in the literature,[1−11] there is a lack of corresponding experimental size distributions, especially for submicron equilibrium vesicles.[1,3] Accurate size distributions of vesicles and other self-assembled submicron structures, while theoretically possible, cannot be obtained with any reliability from light or other scattering methods. Imaging techniques, such as cryo-transmission electron microscopy, provide the most realistic method of obtaining the complete size distribution.[1,2,12,13] However, all electron microscopy techniques can suffer from sample preparation and electron imaging artifacts and need to be reinforced by other methods.

Here we show the similarities and differences between the mean radii, standard deviations, and polydispersities of catanionic equilibrium vesicles measured by cryo-transmission electron microscopy (cryo-TEM), freeze-fracture electron microscopy (FF-TEM), and quasi-elastic light scattering (QLS). We used the size distribution determined from cryo-TEM and a theoretical expression derived from Helfrich elasticity theory and a simple mass action model to determine $K = \kappa + \bar{\kappa}/2$, the sum of the Helfrich mean (κ) and Gaussian ($\bar{\kappa}$) curvature moduli, and R_0, the spontaneous radius of curvature for vesicles made from cetyltrimethylammonium tosylate (CTAT) and sodium dodecylbenzene sulfonate (SDBS). For 7:3 wt CTAT/SDBS at 1% total surfactant in water, $K = \kappa + \bar{\kappa}/2 = 0.15 \pm 0.03\ k_BT$ and $R_0 = 55$ nm $\pm$ 10 nm. For CTAT/SDBS, w/w, at 2% total surfactant, $K = 0.54 \pm 0.05\ k_BT$ and $R_0 = 36$ nm $\pm$ 1 nm. The lower value of K in the CTAT-rich sample is likely due to the hydrophobic tosylate counterion increasing the area per surfactant headgroup.

* To whom correspondence should be addressed. Joseph A. Zasadzinski, Department of Chemical Engineering, University of California, Santa Barbara, Santa Barbara, CA 93106-5080. Phone: 805-893-4769. Fax: 805-893-4731. E-mail: gorilla@engineering.ucsb.edu.

(1) Jung, H. T.; Coldren, B.; Zasadzinski, J. A.; Iampietro, D.; Kaler, E. W. *Proc. Natl. Acad. Sci. U.S.A.* **2001**, *98*, 1353.
(2) Denkov, N. D.; Yoshimura, H.; Kouyama, T.; Walz, J.; Nagayama, K. *Biophys. J.* **1998**, *74*, 1409.
(3) Herve, P.; Roux, D.; Bellocq, A. M.; Nallet, F.; Gulik-Krzywicki, T. *J. Phys. II* (*France*) **1993**, *3*, 1255.
(4) Israelachvili, J. N. *Intermolecular and Surface Forces*, 2nd ed.; Academic Press: London, 1992.
(5) Israelachvili, J. N.; Mitchell, D. J.; Ninham, B. W. *J. Chem. Soc., Faraday Trans. II* **1976**, *72*, 1526.
(6) Bergstrom, M. *Langmuir* **2001**, *17*, 7675.
(7) Bergstrom, M.; Eriksson, J. C. *Langmuir* **1998**, *14*, 288.
(8) Bergstrom, M. *Langmuir* **1996**, *12*, 2454.
(9) Helfrich, W. *Z. Naturforsch.* **1973**, *28c*, 693.
(10) Helfrich, W. *J. Phys.* (*France*) **1986**, *47*, 321.
(11) Safran, S. A.; Pincus, P.; Andelman, D. *Science* **1990**, *248*, 354.
(12) De Smet, Y.; Danino, D.; Deriemaeker, L.; Talmon, Y.; Finsy, R. *Langmuir* **2000**, *16*, 961.
(13) Berclaz, N.; Mueller, M.; Walde, P.; Luisi, P. L. *J. Phys. Chem. B* **2001**, *105*, 1056.

10.1021/la034311+ CCC: $25.00
Published on Web 06/06/2003

We also present a comparison of the cryo-TEM results with QLS measures of the mean hydrodynamic radius and polydispersity and the mean diameter and standard deviation determined from freeze-fracture electron microscopy. The microscopy methods show a surprising agreement in the mean diameter and the standard deviation of the vesicle size distributions, once the fracture process is factored into the size distribution, as both are number-average methods. QLS shows a systematically larger mean vesicle size that is invariant with concentration ratio within a given vesicle lobe. The larger mean size is to be expected as the hydrodynamic radius given by QLS more heavily weights the larger vesicles in the distribution. However, when this weighting is taken into consideration, the mean radius and polydispersity measured by QLS are consistent with that measured by electron microscopy. A second disadvantage of QLS, which is not often appreciated in complex surfactant systems, is that a variety of shapes, such as disks, cylinders, and spheres, may coexist in a surfactant solution. QLS averages over all such shapes, and both the mean radius and polydispersity of each structure might be quite different from the average determined by scattering. The main advantage of QLS is the minimum amount of sample preparation and the quick data accumulation, which makes QLS ideal for initial screens of a large number of samples. However, the combination of QLS, freeze-fracture TEM, and cryo-TEM can provide reliable size distributions of equilibrium vesicles that can then be fit to theoretical expressions to extract bilayer parameters.[1,14]

Materials and Methods

CTAT purchased from Sigma (St. Louis, MO) and SDBS (hard-type) from Tokyo Kasei (Japan) were used as received. Samples were prepared by first mixing stock solutions of the surfactants with Millipore-filtered water to the desired weight fractions. The stock solutions were then combined in the appropriate amounts and allowed several weeks for equilibration. Phase diagrams of the various catanionic vesicle mixtures have been published elsewhere.[15−20] While it is possible to prepare metastable vesicles by shearing lamellar phases,[21,22] there is no indication of a bulk lamellar phase at the concentrations of interest here, nor that shear has influenced the formation or size distribution of the structures shown. Various zero-shear sample preparation methods including dialysis, isothermal counterdiffusion of two micellar dispersions, and in situ surfactant synthesis have shown that catanionic vesicles, including the mixtures of interest here, form independently of the method of sample preparation.[23] Similar catanionic vesicles recover their size distribution after sonication or heat treatment, confirming that the size distribution is an equilibrium feature of the dispersions.[23]

Cryo-TEM. To prepare samples for cryogenic electron microscopy, a thin ($<1\ \mu$m) layer of the surfactant−water mixture was spread on a lacey carbon grid (Ted Pella, Redding, CA) in a temperature-controlled chamber[24] saturated with the solution of interest. The grid was plunged into a mixture of liquid ethane and liquid propane cooled by liquid nitrogen.[25] The frozen samples were transferred to a GATAN (Pleasanton, CA) cold stage and imaged directly at 100 kV using a JEOL 100CXII transmission electron microscope. Bright field phase contrast transmission electron micrographs were recorded using standard low-dose procedures either on film or with a GATAN CCD camera. Vesicle radii were measured from the outer edge of the dark rim in the image to obtain the best representation of the true radius of the vesicle (see Figures 2 and 3). Hundreds of individual vesicles were measured from the digitized images using a commercial image analysis package (Image-Pro Plus version 4.1, Media Cybernetics, Silver Spring, MD) to determine the size distributions. Samples for cryo-TEM were prepared and examined over the course of several weeks to ensure that neither the structures nor the size distributions were changing with time.

Freeze-Fracture Electron Microscopy. Freeze-fracture samples were prepared by first depositing a film of sample liquid approximately 100 microns thick between two copper planchettes. The samples were frozen by plunging the sample into a liquid propane/liquid ethane bath cooled by liquid nitrogen. The frozen sample was transferred under liquid nitrogen to the sample block of a JEM Cryofract freeze-fracture device. The block was then quickly transferred to the vacuum chamber of the Cryofract device via an airlock. After temperature (−170 °C) and pressure ($<10^{-7}$ Torr) equilibration, the sample was fractured and the two resulting surfaces were replicated with approximately 1.5 nm of platinum deposited at a 45° angle, followed by about 15 nm of carbon deposited normal to the surface. The replicas were then removed from the vacuum and warmed to room temperature. The copper planchettes were dissolved in chromerge (a mixture of chromic acid, sulfuric acid, and water), and then the replicas were washed in water and allowed to stand in ethanol for several days to dissolve any remaining surfactant. The replicas were collected on Formvar-coated TEM grids (Ted Pella).[26] A Gatan CCD camera was used to record digital bright field images using a JEOL 100CXII transmission electron microscope. Hundreds of individual vesicles were measured from the digitized images using a commercial image analysis package (Image-Pro Plus version 4.1, Media Cybernetics) to determine the size distributions.

Quasi-Elastic Light Scattering. QLS was performed at 25 °C with a Brookhaven model BI-200SM goniometer, a Brookhaven model BI-9000AT correlator, and a Lexel 300 mW Ar laser. Most experiments were performed at 90°, and the autocorrelation function was analyzed by the method of cumulants.[27] The apparent hydrodynamic radius was obtained from the measured diffusion coefficient using the Stokes−Einstein relationship as described below. The polydispersity index, which is related to the width of the size dispersion, normalized to the mean vesicle size, was determined from the second cumulant of the fit to the autocorrelation function using the software provided with the correlator.

Results and Discussion

The first reported systems of spontaneous "catanionic" vesicles were mixtures of CTAT and SDBS.[15] The tosylate counterion of CTAT is hydrophobic and remains strongly associated with the surfactant aggregate in solution. Inserting the tosylate into the membrane effectively increases the area per surfactant headgroup, which is predicted to reduce membrane rigidity.[18−20,28−30] SDBS

(14) Jung, H. T.; Lee, Y. S.; Kaler, E. W.; Coldren, B.; Zasadzinski, J. A. *Proc. Natl. Acad. Sci. U.S.A.* **2002**, *99*, 15318.
(15) Kaler, E. W.; Murthy, A. K.; Rodriguez, B. E.; Zasadzinski, J. A. N. *Science* **1989**, *245*, 1371.
(16) Kaler, E. W.; Herrington, K. L.; Murthy, A. K.; Zasadzinski, J. A. *J. Phys. Chem.* **1992**, *96*, 6698.
(17) Iampietro, D.; Kaler, E. W. *Langmuir* **1999**, *15*, 8590.
(18) Brasher, L. L.; Herrington, K. L.; Kaler, E. W. *Langmuir* **1995**, *11*, 4267.
(19) Herrington, K. L.; Kaler, E. W.; Miller, D. D.; Zasadzinski, J. A.; Chiruvolu, S. *J. Phys. Chem.* **1993**, *97*, 13792.
(20) Yatcilla, M. T.; Herrington, K. L.; Brasher, L. L.; Kaler, E. W.; Chiruvolu, S. *J. Phys. Chem.* **1996**, *100*, 5874.
(21) Hao, J. C.; Hoffmann, H.; Horbaschek, K. *J. Phys. Chem. B* **2000**, *104*, 10144.
(22) Horbaschek, K.; Hoffmann, H.; Hao, J. *J. Phys. Chem. B* **2000**, *104*, 2781.
(23) McKelvey, C. A.; Hentze, H.-P.; Edlund, H.; Kaler, E. W.; Zasadzinski, J. A. *Langmuir*, submitted.
(24) Bellare, J. R.; Davis, H. T.; Scriven, L. E.; Talmon, Y. *J. Electron Microsc. Tech.* **1988**, *10*, 87.
(25) Chiruvolu, S.; Naranjo, E.; Zasadzinski, J. A. In *Microstructure of Complex Fluids by Electron Microscopy*; ACS Symposium Series, Vol. 578; Herb, C. A., Prud'homme, R. K., Eds.; American Chemical Society: Washington, DC, 1994; p 86.
(26) Zasadzinski, J. A.; Bailey, S. M. *J. Electron Microsc. Tech.* **1989**, *13*, 309.
(27) Koppel, D. E. *J. Chem. Phys.* **1972**, *57*, 4814.
(28) Szleifer, I.; Ben-Shaul, A.; Gelbart, W. M. *J. Phys. Chem.* **1990**, *94*, 5081.
(29) Szleifer, I.; Kramer, D.; Ben-Shaul, A.; Gelbart, W. M.; Safran, S. A. *J. Chem. Phys.* **1990**, *92*, 5081.

(hard-type) is a branched chain aromatic surfactant; such branching can influence hydrocarbon packing in the bilayer interior, which may in turn affect the bending rigidity. It is theoretically predicted that branched hydrocarbons pack more loosely in the bilayer and thus are more accommodating to the gauche hydrocarbon conformations associated with membrane deformations.[28,29] Molecular relaxation (chain rearrangement and flip-flop) in the bilayer could be enhanced by the presence of branched hydrocarbons. Any of these effects could result in a strongly reduced bending rigidity relative to that of equivalent linear chains. However, chain mixing of different surfactants by itself is also predicted to lower the bending rigidity.[28,29]

The ternary phase diagram of CTAT/SDBS/water at 25 °C is dominated by two large and highly stable vesicle lobes for total surfactant concentrations below about 3 wt %. One lobe consists of CTAT-rich vesicles, and the second consists of SDBS-rich vesicles; the vesicle lobes are separated by a precipitate formed at equimolar concentration.[15] The upper limit of surfactant concentration corresponds roughly to the close packing of unilamellar vesicles about 100 nm in size.

Cryo-TEM Results. A quantitative size distribution is necessary to apply theoretical models relating equilibrium vesicle size distributions to fundamental bilayer elastic parameters.[1] Figure 1A shows a representative cryo-TEM image of CTAT/SDBS, 3:7 w/w ratio, at 2 wt % total surfactant in water. In cryo-TEM images, vesicles appear as dark, circular rings on a uniform bright background. The inside of the ring is somewhat darker than the background, and the width of the ring is always greater than the expected bilayer thickness. There are vesicles of many different sizes, as well as some cylindrical in shape, which may be due to slight shearing effects during sample preparation. However, the curvature energy of sufficiently long cylinders is less than that of the equivalent area sphere if there is a finite spontaneous curvature, so coexisting cylinders and spheres may be possible for certain values of the Helfrich elastic moduli.[10,14]

These vesicle images can be easily understood as the projection of the different scattering density of the bilayer relative to the water background. As electrons pass through the sample, they must travel through various lengths of the spherical shell of the vesicle; the fraction of electrons scattered depends on these projected lengths. Near the edge of the vesicle, these projected lengths are large; near the center, the projected length is simply twice the bilayer thickness. The rate of variation of the projection of a spherical shell depends on the shell thickness relative to the shell radius. If the shell thickness is large in comparison to the shell radius, the projection will vary slowly, leading to a low contrast, broad ring. On the other hand, if the shell thickness is small in comparison to the shell radius, the projection will be much higher in contrast and appear much sharper. Simple calculations of the projected thickness of a spherical shell as a function of the radius are shown in Figure 2 for a 4 nm thick bilayer shell, with an inner radius of 80 nm (Figure 2A) or 20 nm (Figure 2B), which are typical of the range of vesicles seen in the images. The absolute contrast should be greater for larger vesicles than smaller vesicles, which is consistent with the images. However, in either case, the apparent width of the ring is significantly greater than the shell thickness. The greatest variation in contrast occurs at the exterior rim of the shell; the change in contrast marks the outside radius of the vesicles and is the best-defined length scale associated with the vesicle. The *absolute* contrast is complicated by phase contrast, defocus, and other imaging effects, but the outer diameter of the dark ring is very close to the true outer diameter of the spherical vesicle.

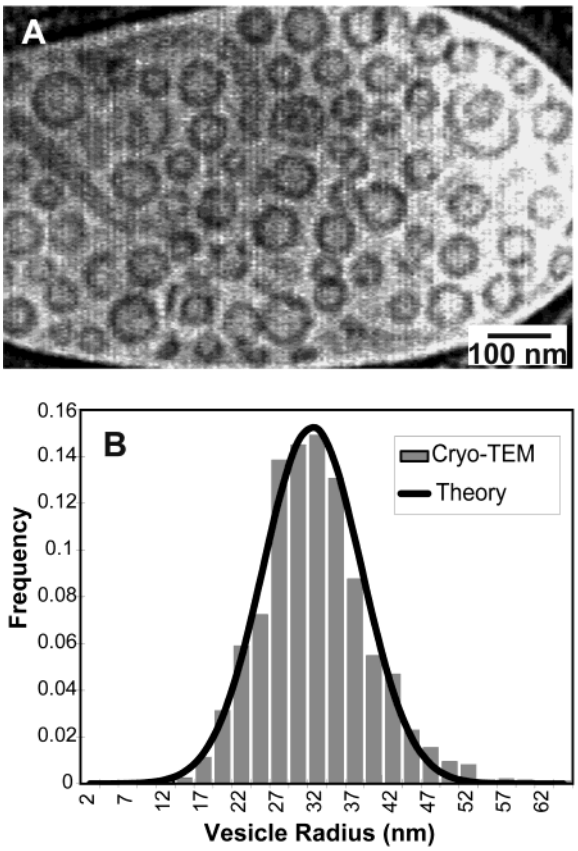

Figure 1. (A) Cryo-TEM image of 3:7 w/w CTAT/SDBS, 2 wt % total surfactant in water at 25 °C. In cryo-TEM images, vesicles appear as dark, circular rings on a uniformly bright background. The area inside the ring is usually somewhat darker than the background. The width of the ring is always greater than the expected bilayer thickness due to the curvature of the vesicle as shown in Figure 2. Extended cylinders are often found in these mixtures and may be due to shear during sample preparation, although they do not appear to be preferentially aligned and their numbers are always low. A sphere to cylinder transition is also possible at equilibrium for certain values of the elastic moduli (ref 14). The nonspherical objects were excluded from the size distributions shown in (B). (B) Histogram of vesicle sizes from cryo-TEM images of CTAT/SDBS, 3:7 w/w, at 2 wt % total surfactant in water. The fit of the bending rigidity model was optimized via the reduced Chi test, giving $R_0 = 36$ nm and $K = 0.54\ k_BT$. On the basis of raw numerical data, the mean vesicle radius was $\langle R \rangle = 30$ nm and $\sigma/\langle R \rangle = 0.32$, which are in excellent agreement with the FF-TEM data. For these broad distributions, the mean vesicle is smaller than the lowest curvature energy vesicle ($\langle R \rangle < R_0$) due to entropy, which favors smaller aggregates.

Figure 1B shows the distribution of the outer vesicle diameter for approximately 2000 vesicles taken from cryo-TEM images of CTAT/SDBS, 3:7 w/w, at 2% total surfactant in water. Consistent with thermodynamic predictions, the distribution is unimodal and roughly Gaussian. The sizes of equilibrium vesicles are determined by a subtle competition between the entropy of vesicle and surfactant mixing and the curvature elasticity of the

(30) Herrington, K. Phase Behavior and Microstructure in Aqueous Mixtures of Oppositely Charged Surfactants. Ph.D. Dissertation, University of Delaware, Newark, DE, 1994.

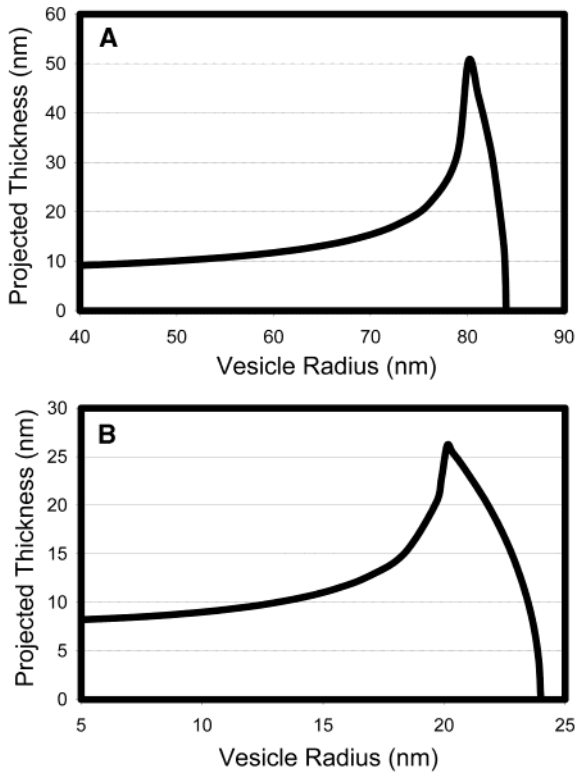

Figure 2. Projected thickness of a spherical vesicle shell 4 nm thick for (A) a spherical shell of 80 nm inside radius and (B) a spherical shell of 20 nm inside radius. Note that the projected length is a maximum at the inside radius of the shell and that the projection tapers off slowly toward the inside of the vesicle. The contrast in cryo-TEM images, while complicated by phase contrast and other electron optical effects, is related to the projected thickness: the greater the thickness, the darker the image. The apparent thickness of the bilayer shell is always greater than the actual thickness of the shell due to the curvature of the bilayer. The most appropriate measurement from cryo-TEM images is to locate where the contrast varies the most, which is the outside radius of the vesicle. Hence, the outer rim of the dark circles in Figure 1 gives an accurate measure of the outside radius of the vesicle.

bilayers.[3,5,31,32] The curvature energy per unit area of bilayer, f_c, is[9,11,33]

$$f_c = \frac{1}{2}\kappa\left(\frac{1}{R_1} + \frac{1}{R_2} - \frac{2}{r_0}\right)^2 + \bar{\kappa}\left(\frac{1}{R_1 R_2}\right) \qquad (1)$$

R_1 and R_2 are the principle radii of curvature; κ is the curvature modulus, and $\bar{\kappa}$ is the saddle-splay modulus. The spontaneous curvature, $1/r_0$, is nonzero only if there is asymmetry between the different sides of the bilayer.[9,11,33] Equation 1 is an appropriate description when the membrane thickness[9,34,35] (here about 3−4 nm[1]) and the Debye length for ionic surfactants[34,36,37] (also about 1−3 nm[1]) are small compared to R_1 and R_2 (about 20−60 nm, see Figure 2). For the spherical vesicles studied here, $R_1 = R_2 = R$, and eq 1 can be simplified:[11,33,38]

$$f = 2K\left(\frac{1}{R} - \frac{1}{R_0}\right)^2$$
$$2K = 2\kappa + \bar{\kappa} \qquad (2)$$
$$R_0 = \frac{2\kappa + \bar{\kappa}}{2\kappa} r_0$$

R_0 is the radius of the minimum curvature energy vesicle (which is different than r_0, the spontaneous curvature radius), and K is an effective bending constant.[11,33] The distribution of surfactant between vesicles of aggregation number M, corresponding to the minimum curvature energy radius, R_0 ($M = 8\pi R_0^2/A_0$, in which A_0 is the mean molecular area), relative to vesicles of aggregation number N and radius R, is dictated by a balance between the entropy of vesicle mixing and the curvature energy, which can be expressed as a mass-action model:[5]

$$\frac{X_N}{N} = \left\{\frac{X_M}{M}\exp\left[\frac{M(\mu_M^0 - \mu_N^0)}{k_B T}\right]\right\}^{N/M} \qquad (3)$$

X_M, μ_M^0 and X_N, μ_N^0 are the mole fraction of surfactant and the standard chemical potential per molecule in vesicles of size M and N, respectively. Equation 3 assumes ideal mixing of the vesicles (not the molecules within the bilayers) and is valid for dilute vesicle dispersions in which the Debye length is small in comparison to the intervesicle distance.[39,40] The chemical potential difference is due to the change in curvature energy per molecule for surfactant distributed between vesicles of different radii:

$$(\mu_N^0 - \mu_M^0) = \frac{4\pi R^2 f}{N} = \frac{8\pi K\left(1 - \frac{R}{R_0}\right)^2}{N} \qquad (4)$$

Inserting eq 4 into eq 3 and substituting $M = 8\pi R_0^2/A_0$ and $N = 8\pi R^2/A_0$ gives the vesicle size distribution as a function of R_0 and K:[1,2,5]

$$C_N = \left\{C_M \exp\left[\frac{-8\pi K}{k_B T}\left(1 - \frac{R_0}{R}\right)^2\right]\right\}^{R^2/R_0^2} \qquad (5)$$

C_M ($=X_M/M$) and C_N are the molar and number fractions of vesicles of size M and N, respectively. A consequence of eq 5 is that vesicles with $K \sim k_B T$ have a much broader size distribution than vesicles with $K \gg k_B T$. This is the opposite of vesicle size distribution models that do not include a spontaneous curvature.[3,4] A best fit of eq 5 to the size distribution of CTAT/SDBS, w/w, at 2% total surfactant measured by cryo-TEM results in $K = 0.54 \pm 0.05$ $k_B T$ and $R_0 = 36 \pm 1$ nm, with a reduced Chi test = 1.8 (Figure 4). On the basis of the raw numerical data, the mean vesicle radius $\langle R\rangle = 30$ nm and $\sigma/\langle R\rangle = 0.32$.

A cryo-TEM image of 7:3 w/w CTAT/SDBS at 1 wt % total surfactant in water is shown in Figure 3A. Figure 3B shows the vesicle size distribution generated from this and other cryo-TEM images of about 2000 vesicles. The distribution of sizes is unimodal and was fit to eq 5 to

(31) Morse, D. C.; Milner, S. T. *Phys. Rev. E* **1995**, *52*, 5918.
(32) Simons, B. D.; Cates, M. E. *J. Phys. II* (*France*) **1992**, *2*, 1439.
(33) Safran, S. A.; Pincus, P. A.; Andelman, D.; MacKintosh, F. C. *Phys. Rev. A* **1991**, *43*, 1071.
(34) Dubois, M.; Zemb, T. *Curr. Opin. Colloid Interface Sci.* **2000**, *5*, 27.
(35) Safran, S. A. *Statistical Thermodynamics of Surfaces, Interfaces and Membranes*; Addison-Wesley: Reading, MA, 1994.
(36) Fogden, A.; Ninham, B. W. *Adv. Colloid Interface Sci.* **1999**, *83*, 85.
(37) Fogden, A.; Carlsson, I.; Daicic, J. *Phys. Rev. E* **1998**, *57*, 5694.
(38) f_c and f are related by a constant term independent of the vesicle curvature.
(39) The minimum ionic strength of these catanionic solutions is equal to the concentration of the minor surfactant component, and the maximum is the total surfactant concentration. For these experiments, the ionic strength ranges from about 10−100 mM. This leads to a Debye length of 1−10 nm (see Chapter 12 of ref 4), a small fraction of the average intervesicle spacing (as seen in the micrographs) of 75−100 nm. Hence, electrostatic interactions are negligible between the vesicles and the ideal mixing approximation is justified.
(40) Chiruvolu, S.; Israelachvili, J.; Naranjo, E.; Xu, Z.; Kaler, E. W.; Zasadzinski, J. A. *Langmuir* **1995**, *11*, 4256.

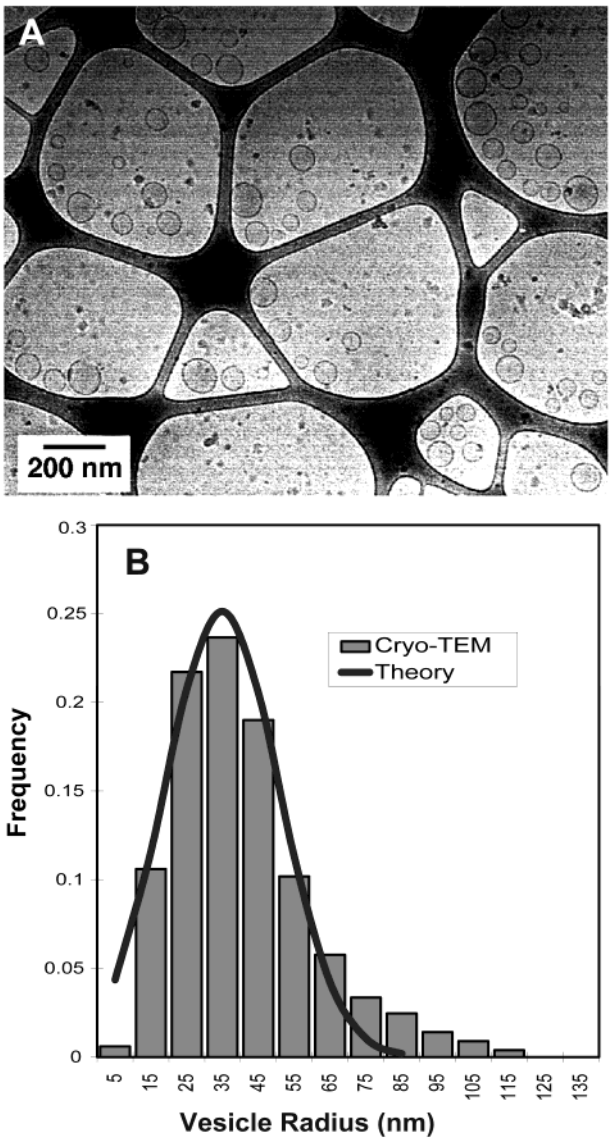

Figure 3. (A) Cryo-TEM image of 7:3 w/w CTAT/SDBS, 1 wt % total surfactant in water at 25 °C. Only spherical vesicles are observed, and they are larger and more broadly size disperse than the SDBS-rich vesicles in Figure 1. Small black spots are frost contamination. (B) Histogram of vesicle sizes from cryo-TEM images of CTAT/SDBS, w/w, at 2 wt % total surfactant in water. The fit of the bending rigidity model was optimized via the reduced Chi test, giving $R_0 = 55$ nm and $K = 0.15\ k_BT$. On the basis of raw numerical data, $\langle R\rangle = 43$ nm and $\sigma/\langle R\rangle = 0.59$, which are again in excellent agreement with the corresponding FF-TEM data.

determine that the optimized $K = 0.15 \pm 0.03\ k_BT$, and $R_0 = 55 \pm 10$ nm, with a reduced Chi test = 2.3. The uncertainty in R_0 is quite high when working with such broad distributions because the model is only weakly sensitive to R_0. The relatively poor fit quality also can be attributed to the mismatch between theory and experiment for $R < 10$ nm. The simple Helfrich theory does not account for higher order curvature terms that are important when the bilayer radius is only a few multiples of the bilayer thickness. On the basis of raw numerical data, $\langle R\rangle = 42.6$ nm and $\sigma/\langle R\rangle = 0.59$. For these broad distributions, $R_0 > \langle R\rangle$, as entropy favors smaller aggregates.[4,5]

Comparison of Mean Vesicle Sizes Measured by QLS and Cryo-TEM. Although the data are difficult to interpret quantitatively, QLS is a convenient tool for quickly comparing vesicle sizes when dealing with a large number of samples. In addition, QLS does not require any special sample preparation except for filtering dust and other particles. The vesicle sizes we observed by QLS are generally in good agreement with vesicle samples of similar compositions published previously.[16] For both CTAT-rich and SDBS-rich vesicles within each vesicle lobe, there is no variation in vesicle size with SDBS/CTAT ratio. For CTAT-rich vesicles, we observe a hydrodynamic radius $R_{QLS} = 57 \pm 2$ nm, and a polydispersity index (PI) of 0.25 ± 0.03. For SDBS-rich vesicles, $R_{QLS} = 49 \pm 3$ nm and PI $= 0.2 \pm 0.03$. The lack of size dependence with composition is consistent with the idea that the actual vesicle bilayer composition is relatively fixed and that excess anionic or cationic surfactant is expelled to coexisting micelles or solution.[30] It also suggests that the bilayer elastic parameters and spontaneous curvature do not depend on composition within a vesicle lobe. The polydispersity index is a rough measure of the width of the size distribution, normalized to the mean hydrodynamic radius, but should not be confused with the standard deviation of the distribution.[27] Qualitatively, the QLS data agree with both the cryo-TEM results that show the SDBS-rich vesicles to be smaller and more monodisperse than the CTAT-rich vesicles. However, the hydrodynamic radius measured by QLS is significantly larger than the number-average radius measured by both cryo-TEM and FF-TEM.

This is because QLS does not give a number-average mean radius; rather, the hydrodynamic radius measured by QLS is skewed toward larger sizes due to the dependence of the scattering intensity on the size of the object. The intensity of the scattered light from a vesicle with a mass M_i is proportional to M_i^2. QLS measures the z-averaged diffusion coefficient, D_z, as[41]

$$D_z = \frac{\sum_i x_i M_i^2 D_i}{\sum_i x_i M_i^2} \tag{6}$$

where x_i is the number fraction of vesicles of radius i, M_i is the mass of size i, and D_i is the diffusivity of size i. For a vesicle, M_i is proportional to R_i^2 as the vesicle is a hollow shell. Hence,

$$D_z = \frac{\sum_i x_i R_i^4 D_i}{\sum_i x_i R_i^4} \tag{7}$$

and inserting the Stokes−Einstein relation between size and diffusivity, $D_i = k_BT/(6\pi\mu R_i)$, we have

$$D_z = \frac{k_BT}{6\pi\mu} \frac{\sum_i x_i R_i^3}{\sum_i x_i R_i^4} \tag{8}$$

The mean hydrodynamic radius, R_{DLS}, can be extracted

(41) Berne, B. J.; Pecora, R. *Dynamic Light Scattering*; J. Wiley and Sons: New York, 1976.

from this expression for D_z by again using the Stokes–Einstein relation, $R_{hyd} = k_B T/(6\pi\mu D_z)$, yielding

$$R_{hyd} = \frac{\sum_i x_i R_i^4}{\sum_i x_i R_i^3} \tag{9}$$

From eq 9, the hydrodynamic radius can be approximated as the fourth moment of the vesicle size distribution divided by the third moment. While it is impossible to determine the full size distribution from QLS to compare to the cryo-TEM size distributions, the hydrodynamic radius can be calculated from the size distribution measured by cryo-TEM.

For the CTAT-rich vesicles, the number-average radius determined from the cryo-TEM images is $\langle R\rangle = 43$ nm. From the size distribution in Figure 3B, we can use eq 9 to calculate an equivalent hydrodynamic radius, $R_{hyd} = \sum_i x_i R_i^4/\sum_i x_i R_i^3 = 63$ nm, which is close to the $R_{QLS} = 57 \pm 2$ nm measured by QLS. The calculated hydrodynamic radius is very sensitive to the fraction of the largest vesicles; if the largest 1% of vesicles in the cryo-data is left out of the calculation, R_{hyd} drops to 59 nm. Hence, while QLS can clearly give a consistent measure of the average radius, this average should always be greater than that determined by TEM and is dominated by any large particles that may be in the solution. For the SDBS-rich solution, the number-average radius of the spherical vesicles is $\langle R\rangle = 30$ nm. From Figure 1B and eq 9, $R_{hyd} = \sum_i x_i R_i^4/\sum_i x_i R_i^3 = 37$ nm, which is quite a bit smaller than the 49 ± 3 nm measured by QLS. This discrepancy points out a limitation of QLS relative to direct imaging. In the cryo-TEM images, Figure 1A, of the SDBS-rich solutions, there are long, cylindrical bilayer aggregates in addition to the spherical vesicles. QLS gives an average hydrodynamic radius for all of the structures in solution; the cylindrical vesicles likely skew the mean size and the polydispersity toward larger values.

Freeze-Fracture Results. Size distributions from cryo-TEM samples can be complicated by vesicle segregation during sample preparation. The water film in a cryo-TEM sample varies in thickness from a few microns to a few hundred nanometers over the TEM grid, thicker near the supporting holey polymer films of the grid and thinner in the gaps between the polymer films. This should not significantly affect the size distributions shown in Figures 1A and 3A as the vesicles are small compared to all the sample thickness. However, to confirm the cryo-TEM size distributions, it is useful to compare the mean radius and standard deviation between samples that have the same mean radius and polydispersity when measured by QLS by a technique that does not require such thin water films. Hence, we used freeze-fracture to measure the size distribution in samples with slightly different composition, but that had the same mean radius and polydispersity as measured by QLS.

However, evaluating a mean vesicle size from a freeze-fracture electron microscopy image is complicated by the fracture process. In freeze-fracture, vesicles appear as hemispherical domes or craters with distinct shadows (absence of platinum). The fracture plane can pass through any part of the vesicle, skewing the apparent size distribution toward smaller sizes. By accounting for the probability density of cross fracture planes, Hallett et al.[42] determined simple corrections to give better estimates of the mean and standard deviation of a spherical vesicle distribution. In a freeze-fracture replica, fractured vesicles can be interpreted as the intersection of a random fracture plane with a sphere of radius R. The image then appears in the micrograph as a circle of radius $r \le R$. If the cleavage plane is equally probable at all positions within the vesicle, the probability that the apparent radius in the image is between r and $r + dr$ is $G(r)\,dr$, which, for a vesicle of radius R, is[42]

$$G(r) = \frac{r}{R(R^2 - r^2)^{1/2}} \tag{10}$$

If $H(R)$ is the actual vesicle size distribution, then the apparent distribution of radii determined from a freeze-fracture image is $I(r)$:

$$I(r) = \int_r^\infty \frac{r}{R(R^2 - r^2)^{1/2}} H(R)\,dR \tag{11}$$

The integration goes from r to ∞ because the true vesicle radius, R, is never smaller than the apparent radius on the freeze-fracture image, r. As can be seen from eq 11, evaluating the size distribution requires a priori knowledge of the functional form of the distribution. Even if we assume the functional form given by our spontaneous curvature theory, eq 5, a complete deconvolution of the freeze-fracture size distribution is a practical impossibility. Fortunately, the first two moments of the size distribution can be determined from FF-TEM data *independent* of any functional form of the actual size distribution. Since

$$\langle r\rangle = \int_0^\infty rI(r)\,dr = \int_0^\infty H(R)\left[\int_0^R \frac{r^2}{R(R^2 - r^2)^{1/2}}\,dr\right]dR \tag{12}$$

$$\langle r\rangle = \frac{\pi}{4}\int_0^\infty RH(R)\,dR = \frac{\pi}{4}\langle R\rangle$$

eq 12 relates the mean radius measured from the freeze-fracture images, $\langle r\rangle$, with the true mean radius of the distribution, $\langle R\rangle$: $\langle R\rangle = 4\langle r\rangle/\pi$. By determination of the average apparent radius of the fractured vesicles, the average vesicle radius can be calculated by a simple multiplicative factor.

The standard deviation of the vesicle radii can also be determined from the freeze-fracture images in a similar way. The second moment of $I(r)$ yields the mean square value, $\langle r^2\rangle$:

$$\langle r^2\rangle = \int_0^\infty r^2 I(r)\,dr = \int_0^\infty H(R)\left[\int_0^R \frac{r^3}{R(R^2 - r^2)^{1/2}}\,dr\right]dR \tag{13}$$

$$\langle r^2\rangle = \frac{2}{3}\int_0^\infty R^2 H(R)\,dR = \frac{2}{3}\langle R^2\rangle$$

From eqs 12 and 13, the standard deviation of the vesicle size distribution can be easily calculated:

$$\sigma^2 = \langle R^2\rangle - \langle R\rangle^2 = \frac{3}{2}\langle r^2\rangle - \frac{16}{\pi^2}\langle r\rangle^2 \tag{14}$$

Although freeze-fracture images cannot easily give a complete representation of the vesicle size distribution, the mean and standard deviations of the size distribution can be compared between the cryo-TEM and freeze-fracture sample preparations. As freeze-fracture samples

(42) Hallet, F. R.; Nickel, B.; Samuels, C.; Krygsman, P. H. *J. Electron Microsc. Tech.* **1991**, *17*, 459.

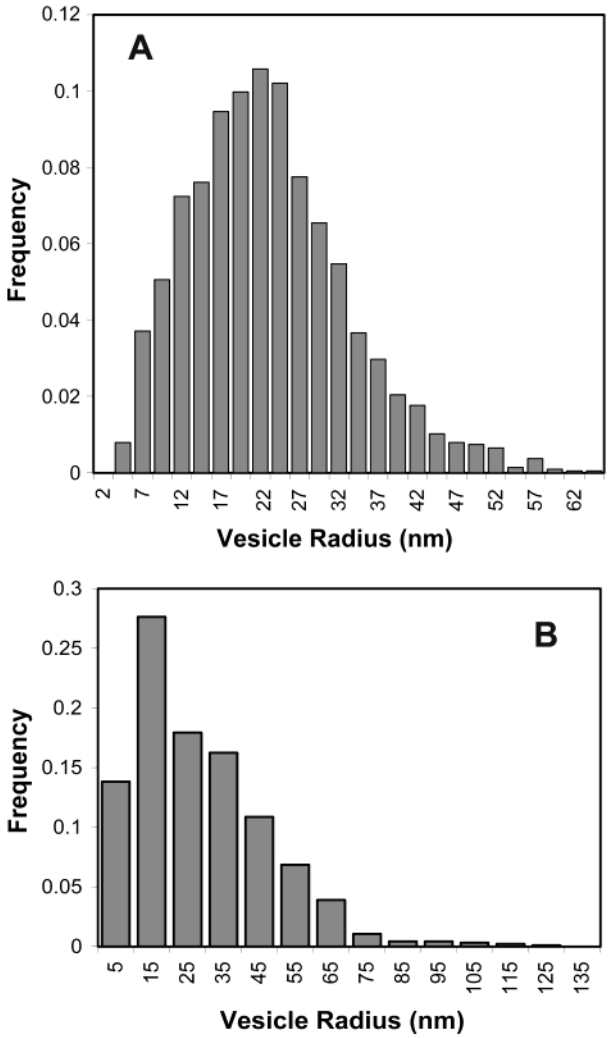

Figure 4. (A) Histogram of vesicle sizes from freeze-fracture TEM images (not shown) of 2:8 w/w CTAT/SDBS, 2 wt % total surfactant in water at 25 °C, uncorrected for the effect of random fracture planes in the FF-TEM image. After correction, $\langle R\rangle$ = 30 nm and $\sigma/\langle R\rangle$ = 0.34, in excellent agreement with the corresponding cryo-TEM size distributions of the SDBS-rich vesicles (Figure 1A). (B) Vesicle size distribution histogram from FF-TEM images (not shown) of 8:2 w/w CTAT/SDBS at 1 wt % total surfactant at 25 °C. Sizes are raw FF-TEM data, uncorrected for the effect of random fracture planes, and thus are skewed to smaller sizes. After correction, $\langle R\rangle$ = 37 nm and $\sigma/\langle R\rangle$ = 0.59, which are in good agreement with cryo-TEM data above. Apparently, neither the small difference in vesicle composition nor the FF-TEM deconvolution introduces significant errors. The two sets of images were generated years apart from different surfactant stocks.

are typically 10−100 microns thick, problems of size segregation, compression, and orientation that trouble cryo-TEM are not present in freeze-fracture. While both techniques may suffer from freezing artifacts (which are minimized in cryo-TEM samples due to their smaller thickness and can be evaluated by diffraction to determine if there has been ice crystal formation, see refs 25 and 26), freeze-fracture samples are not damaged by electron beam irradiation, and the contrast in the image is generated by different processes. Hence, agreement between the two methods is good evidence that the size distributions determined by both methods are accurate.

Figure 4 shows vesicle size distribution histograms determined from freeze-fracture TEM images (not shown) for CTAT/SDBS, 2:8 w/w at 2 wt % (Figure 4A) and 8:2 w/w at 1 wt % total surfactant in water at 25 °C (Figure 4B). The size distribution shows the apparent vesicle radius, uncorrected for the effect of random fracture planes, and thus is skewed to smaller sizes. Figure 4A shows CTAT/SDBS 2:8 w/w at 2 wt % total surfactant in water at 25 °C. The corrected $\langle R\rangle$ = 30 nm and $\sigma/\langle R\rangle$ = 0.34 are in excellent agreement with cryo-TEM of CTAT/SDBS 3:7 w/w at 2% total surfactant of $\langle R\rangle$ = 30 nm and $\sigma/\langle R\rangle$ = 0.32. For the 8:2 w/w CTAT/SDBS at 1 wt % total surfactant in water at 25 °C, the apparent size distribution is shown in Figure 4B. As expected from the random fracture planes, the distribution is biased toward smaller radii than the cryo-TEM distributions. After deconvolution, $\langle R\rangle$ = 37 nm and $\sigma/\langle R\rangle$ = 0.59, in good agreement with the cryo-TEM which gave $\langle R\rangle$ = 43 nm and $\sigma/\langle R\rangle$ = 0.59. As discussed previously, QLS shows that the hydrodynamic radius and polydispersity do not change significantly with composition over this range, so this good agreement speaks to the consistency between all three methods of measuring the size distribution. Apparently, neither the small difference in vesicle composition nor the FF-TEM deconvolution introduced significant errors. Furthermore, the two sets of images were generated years apart from different surfactant stocks, indicating the repeatable properties of these thermodynamically controlled vesicle systems.

For both vesicle compositions in the CTAT/SDBS/water system, cryo-TEM and FF-TEM size distributions are in excellent agreement once $\langle R\rangle$ and $\sigma/\langle R\rangle$ are properly scaled. However, cryo-TEM remains the only technique for unambiguously determining the full size distribution of polydisperse fluctuating vesicles and, hence, estimating elastic properties. Nevertheless, FF-TEM is clearly a reliable tool for determining $\langle R\rangle$ and $\sigma/\langle R\rangle$ as well as verifying a unimodal vesicle size distribution. Furthermore, FF-TEM shares cryo-TEM's advantages over scattering in the ability to ignore dust and generate number-average data rather than higher moment averages. There are even advantages of FF-TEM over cryo-TEM: a much lower probability of shear-induced artifacts and artifacts due to evaporation/condensation. Thus, FF-TEM and cryo-TEM should be viewed as complementary techniques that should be used in parallel to generate unambiguous colloidal size distributions.

Conclusions

Cryo-TEM, freeze-fracture TEM, and quasi-elastic light scattering are complementary methods to determine mean radii, polydispersity, and even the complete size distribution of submicron colloidal particles including spontaneous vesicles. Cryo-TEM and FF-TEM show surprising agreement in both the mean radii and the standard deviation of both CTAT-rich and SDBS-rich spontaneous vesicle samples, once the FF-TEM data are corrected for the fracture process. Moreover, both are number-average methods so they generally are more suitable for comparison to theoretical size distributions. QLS shows a systematically larger mean vesicle size, but comparisons of the relative sizes and polydispersities between the CTAT-rich and the SDBS-rich samples are consistent with both microscopy methods. For the CTAT-rich samples that only form spherical vesicles, the cryo-microscopy data, when weighted appropriately for the scattering intensity, give a mean radius in good agreement with the hydrodynamic radius measured by QLS. However, the agreement is less good for the SDBS-rich sample. This points out a disadvantage of QLS that is not often appreciated in complex surfactant systems. Surfactant aggregates can take on a variety of shapes including disks, cylinders, and spheres. QLS averages over all such aggregates in solution,

and both the mean radius and polydispersity of each structure might be quite different from the average hydrodynamic radius. The main advantage of QLS is the minimum amount of sample preparation and the quick data accumulation, which makes QLS ideal for initial qualitative comparisons between large numbers of samples. However, the combination of QLS, freeze-fracture TEM, and cryo-TEM can provide reliable size distributions of equilibrium vesicles that can then be fit to theoretical expressions to extract material parameters.

With the exception of systems containing longer fluorinated chains (>7 carbons),[1] equilibrium vesicles formed from catanionic surfactant mixtures of unequal chain length are typically polydisperse. Within the confines of our thermodynamic model incorporating spontaneous curvature, this would indicate that these catanionic surfactant mixtures form bilayers of very low rigidity (of order k_BT) regardless of differences in headgroup chemistry (sulfate, sulfonate, carboxylate, etc.), counterion (bromide, chloride, tosylate, etc.), chain length (6−16 carbons), and degree of branching (SDBS). The tosylate counterion in the CTAT/SDBS system also leads to a decrease in the effective bilayer rigidity. For SDBS-rich bilayers, the effective elastic constant $K = 0.54\ k_BT$, which is similar to that of linear-chain bilayers in cetyltrimethylammonium bromide (CTAB)/sodium octyl sulfate (SOS) and CTAB/FC5, which also have $K \sim 0.5\ k_BT$.[1] Hence, it appears that hydrocarbon branching does not reduce membrane rigidity significantly over simple chain mixing. However, CTAT-rich vesicles have an effective elastic constant $K = 0.15\ k_BT$, significantly lower than those of CTAB/SOS, CTAB/FC5, *or* SDBS-rich bilayers. In fact, it is similar to that of equimolar dodecyltrimethylammonium chloride (DTAC)/SOSo bilayers ($K = 0.12\ k_BT$, to be published). Since the DTAC/SOSo bilayers comprise fully dissociating hydrophilic counterions and much shorter unbranched chains, we may conclude that the tosylate counterions in CTAT-rich bilayers probably do remain associated with the bilayer, increase the area per surfactant head, and dramatically reduce the measured rigidity. In that case, the role of tosylate in the bilayer is analogous to that of short-chain fatty alcohols that also promote the reduction in measured membrane rigidity.[43] Hence, it appears that much of the reduction in bilayer elasticity common to spontaneous vesicle bilayers is due to simple chain mixing, regardless of the type of chain being mixed. However, increasing the area of the headgroup can reduce the elasticity even more, leading to more polydisperse vesicle populations.

Acknowledgment. The authors thank J. Israelachvili and E. Kaler for ongoing collaborations and discussions and Dr. D. Danino for training R.V.Z. in cryo-microscopy techniques. The authors gratefully acknowledge support by National Institutes of Health Grant EB-00380 and National Science Foundation Grant CTS-9814399 and the use of equipment supported by the NSF MSERC Program.

LA034311+

(43) Chiruvolu, S.; Warriner, H. E.; Naranjo, E.; Idziak, S.; Radler, J. O.; Plano, R. J.; Zasadzinski, J. A.; Safinya, C. R. *Science* **1994**, *266*, 1222.